

Forced wetting of hydrophobic knitted fabrics analyzed with X-ray imaging

Florence Biguenet¹, Rolf Stämpfli², Sascha Krügl¹, Téo Georges², Dominique Dupuis¹, René M Rossi² and Marie-Ange Bueno¹

¹Université de Haute Alsace, Laboratoire de Physique et Mécanique Textiles (LPMT UR 4365), Ecole Nationale Supérieure d'ingénieurs Sud Alsace, France

²Empa, Swiss Federal Laboratories for Materials Science and Technology, Laboratory for Biomimetic Membranes and Textiles, Switzerland

Abstract:

Understanding how water droplets penetrate a textile fabric under forced conditions is of considerable interest for sportswear comfort and protective clothing, but also for processes such as inkjet printing. Investigations on the role of geometrical morphology in liquid transport face difficulties in identifying the relevant geometrical parameters at play. Here, X-ray tomography was used to investigate how the liquid distributes inside knitted fabrics when a droplet is squeezed onto its surface using a specifically developed device. It makes it possible to visualize the dynamics of the droplet's penetration and to analyze the final liquid distribution after releasing the compression. The three-dimensional liquid zone can be reconstructed with a specific method and qualitatively analyzed. Variation in hydrophobicity and porosity, characterized by the cover factor, is the main contributor to changes in liquid distribution among samples, by influencing in-plane spread, i.e. on the surface, and/or transplanar spread, i.e. penetration into the thickness of the fabric.

Keywords: wetting, in-plane and transplanar penetration, hydrophobic knit, X-ray tomography.

1. INTRODUCTION

Fundamental knowledge of the interaction between a liquid and a fibrous material is important for many key processes in the textile industry and textile end uses. However, the complex mechanisms involved are still incompletely understood and are the subject of an active research field. Numerous, partly standardized testing methods enable the evaluation of wetting or wicking properties of textile materials thanks to specific parameters. The in-plane liquid transport properties of fabrics may be easily tested by vertical or horizontal wicking tests using visual or gravimetric measurements. Two experimental techniques are commonly performed: the strip test and the spot test (1–4). These tests are the basis for several standards (DIN 53924, AATCC 195, AATCC 197, AATCC 198, ISO 22608, ISO 9073-6). The transplanar transport properties of fabrics are less precisely evaluated by measuring, for example, the time required

for liquid to infiltrate through the fabric (such as EN 20811, AATCC 198, ISO 9073-8, ISO 7198) or the quantity of liquid contained in the wetted area (gravimetric measurements (5,2,6), visual measurements (7,8), electrical resistance measurements (9–11)).

Predicting imbibition in a porous media is usually done by referring to Darcy's law or the Lucas–Washburn equation (12,13). The parameters characterizing the topographic porous network are permeability for the first law and an equivalent porous radius for the second. Even though these equations generally reflect the time-dependent behaviors observed, the determination of the topographic parameters (pore tortuosity, interconnections, homogeneity, dimensional dispersion, regularity...) from direct observation of the pore geometry are arduous (14,15).

The complexity of the investigations on the role of geometrical morphology in predicting liquid transport are exemplified for textile materials as classical porous media (1,5,16,17). Indeed, most fabrics involve several length scales from sub-micrometer to millimeter that are all relevant to wetting and wicking mechanisms. Common parameters considered can be listed: material (composition), shape of fiber, twist of yarn, yarn structure, yarn count, hairiness, fabric weight, thickness, porosity, stitch length, cover factor (3,4), kind of knit, chemical or physical treatments. Some of these parameters are dependent on the others, which increases the complexity of investigating their influence on wetting properties. An additional challenge for porous substrates formed by an assembly of particles (fibers, sand) is the change in pore geometry during penetration due to swelling or particle movement induced by capillary forces (18).

Many textile processes such as sizing, coating, finishing and printing consist in forcing the liquid into the textile fabric. Many other applications involve this process. For example, as superhydrophobic textile surfaces are of considerable interest for many applications, the robustness of this property under mechanical constraints needs to be guaranteed. It can be tested by squeezing a droplet under the superhydrophobic surface (19). More common examples concern wear comfort, especially for evacuation of sweat by compression sportswear or protective clothing (20). Textile printing implies projecting droplets onto textile surfaces (15,21). In this case, the understanding of the phenomena involved has to be improved for ecological and economic considerations (for silver-based inks, for example).

For both spontaneous and forced transport mechanisms, a common problem limiting understanding is the lack of information about the microscopic pore geometry. The mechanisms, operating at both macro- and microscales cannot be understood based on traditional measurement techniques. To visualize liquid distribution in an opaque fabric, Bencsik *et al.* (22) employed Nuclear Magnetic Resonance. The distribution of liquid through the textile thickness was analyzed, but the in-plane distribution within the textile was not considered. High-resolution X-ray imaging enables the visualization of the pore space (23), the interfaces (24,25) and water position during spontaneous wetting in a textile structure (26,27). Commercial X-ray computed tomography (μ CT) scanners provide broader information in three dimensions on subsurface liquid transport phenomena (28–31).

Based on X-ray imaging and tomography, this paper presents a new method to investigate forced wetting inside knit fabrics. The relevance of this method is illustrated with hydrophobic textile structures by analyzing the role of hydrophobicity and of different geometrical knit parameters on liquid distribution. Forced wetting is performed by squeezing a water droplet on

the textile surface using a newly developed specific loading cell. Two specific scenarios have been defined: a 2D imaging (projection) for a vertical view during the compression-decompression cycle of the textile and a 3D scanning (tomography) of the liquid distribution inside the fabric after decompression.

2. MATERIALS AND METHODS

2.1 Fabric samples

Various knitted fabrics were specifically produced to analyze the influence of levels of hydrophobicity and porosity, i.e. in the present case the inverse of the cover factor. Cover factor (CF) is defined as the ratio of the yarn diameter and the stitch length (SL) in centimeters per stitch. The yarn diameter is proportional to the square root of the yarn count (t) in tex, therefore the cover factor can be simplified as (32).

$$CF = \frac{\sqrt{t}}{SL} \quad (1)$$

A Jacquard flat knitting machine (Stoll ADF BW 32, Reutlingen, Germany) was used, varying one parameter at a time to enable systematic comparison (Table 1):

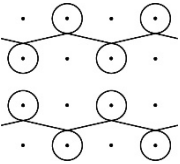
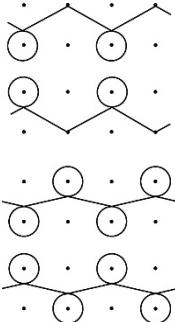
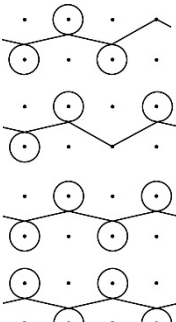
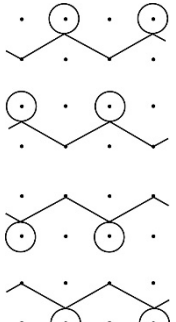
- The stitch length, i.e. the yarn length necessary to form a stitch, modifies the cover factor value for a given kind of yarn and kind of knit (Eq. 1);
- The number of yarns (one, two or three) allows the cover factor to be varied by changing the total yarn count (Eq. 1) since the yarns are knitted together as a thread at constant stitch length;
- The kind of knit chosen was interlock and the main knitted structure used is interlock 1 and 1 (Table 2);
- Some samples were given a hydrophobic treatment, as indicated in Table 1.

Table 1: Investigated knitted fabric characteristics. The sample code refers to material (1 for acrylic and 4 for cotton), hydrophobic treatment (a is without, b with treatment), stitch length (10 to 14 corresponding to the machine process, for 6.8 to 11 mm/stitch), kind of knit (no information for interlock 1x1 and P1 to P3 for the other patterns described in Table 2), number of knitted yarns (F1 to F3 for 1 to 3 yarns).

Reference	Yarn	Stitch length (mm)	Number of yarns	Kind of knit	Hydrophobic treatment	Thickness (mm)	Cover factor (tex ^{1/2} .cm ⁻¹)
1b10	Acrylic 65 tex	6.8	1	1x1 Interlock	With	2.66±0.02	11.9
1a10					Without	2.66±0.02	
1a11						2.87±0.06	
1a12						2.96±0.08	
1a13						3.06±0.09	
1a14		3.13±0.04					
1a10-P1		3.01±0.11		N/A			
1a10-P2		3.00±0.08					
1a10-P3		3.94±0.14					
1a12-F2		8.7	2				3.30±0.02

1a14-F2		11.0		1x1 Interlock		3.68±0.04	10.4
4b10-F1	Cotton 28 tex	6.8	1	1x1 Interlock	With	2.06±0.08	7.9
4b10-F2			2			2.22±0.02	11.1
4b10-F3			3			2.78±0.11	13.6

Table 2: Interlock knit kinds investigated.

1x1 Interlock	P1	P2	P3
			

A preliminary study using fabrics made from multi-filament PET yarns failed to retain liquid and the droplet was not visible on the μ CT images after compression. Therefore, all the fabrics used were made from staple fiber yarns and presented superficial hairiness. Most of the knitted fabrics investigated were made from an acrylic ply yarn with a count of 65 tex (Table 1). The other fabrics were made from a 28 tex cotton yarn.

The chosen knitted fabrics had sufficient thickness, i.e. at least 2 mm, and density to be able to characterize the 3D water distribution by X-ray. The kinds of knits were based on interlock, and most of the fabrics investigated were interlock 1 x 1 because this pattern is very common and gives a very dense structure. The other patterns (P1-P3) were derivatives of interlock 1 x 1, but with different structures.

Some fabrics are functionalized by a chemical hydrophobic treatment (Table 1), obtained by a commercial C6-based treatment (4% wt Nuva® N1811, Archroma). The process used is bath and padding. This treatment modifies i) acrylic fabrics, which are initially slightly hydrophobic, to become strongly hydrophobic, ii) cotton fabrics, which are initially hydrophilic and hygroscopic, to become hydrophobic. In terms of water contact angle on the knitted fabrics, no difference can be observed before or after this treatment for spontaneous wetting due to yarn hairiness (Fig 1a and b). However, in terms of capillary rise in treated and non-treated yarns, a significant different quantity of liquid uptake can be observed for a liquid composed of 50% water and 50% ethanol (Fig.1c).

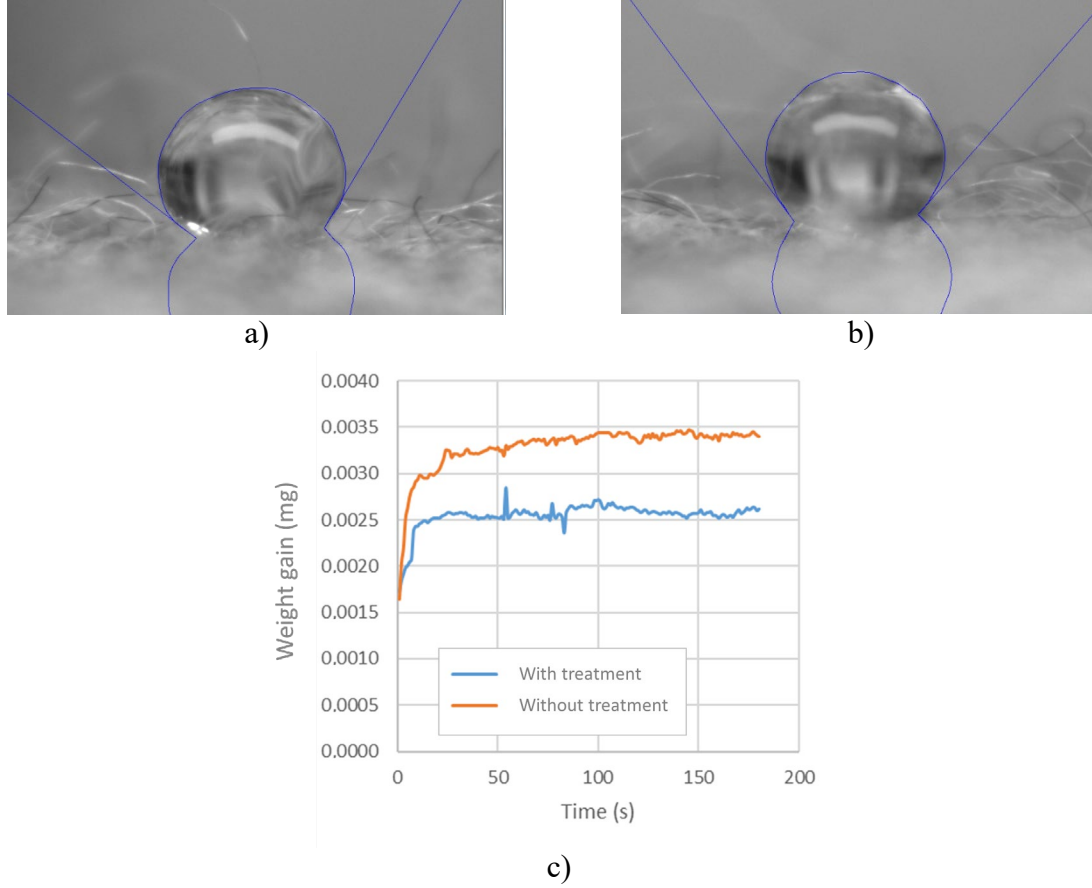


Figure 1: Droplet a) without and b) with hydrophobic treatment for acrylic knitted samples, respectively 1a10 and 1b10 (Table 1) and c) capillary rise for the corresponding yarns.

2.2 X-ray microcomputed imaging and tomography (μ CT)

Computerized tomography is a layer-selective radiographic process, by which a three-dimensional image can be reconstructed with the aid of a number of sectional radiographs. Each projection corresponds to the integration of the attenuation coefficient along the X-ray beam, and, by combining the data from different angles, it is possible to reconstruct a three-dimensional image of a sample. The μ CT scanner used for our investigations was an industry tabletop model (μ CT 80) from Scanco Medical AG (Brüttisellen, Switzerland). The experimental settings are given in Table 3.

Table 3: Experimental settings for x-ray tomography and imaging

Setting	Tomography (3D)	Projections (2D time series)
X-ray anode voltage	70 kV peak	70 kV peak
X-ray anode current	114 μ A	114 μ A
Projections	500	1
Integration time per projection	217 ms	317 ms
Resolution	1024 x 1024	1024 x 128
Edge length	74 μ m (voxel)	37 μ m (pixel)
Slices	104 (2 stacks of 52)	—
Measurement time	10 min	2.86 s/frame (2 stacks)

The laboratory is air-conditioned at a temperature of $20^{\circ}\text{C} \pm 2^{\circ}\text{C}$ and a relative humidity of $65\% \pm 5\%$. Due to heat generation by the X-ray tube, the climate within the instrument is $23.5^{\circ}\text{C} \pm 1.5^{\circ}\text{C}$ and $57\% \pm 5\%$, respectively.

Since computed tomography is time-consuming, it is only suitable for observing slow dynamic processes. Therefore, the experiment was divided into two phases. In the first phase, which consisted of compression and release, a time series of individual projections was used to obtain an image every 3 s. In the second phase, tomography was used to get a 3D visualization of the liquid distribution inside the fabric after decompression.

2.3 Specific compression device

To support the samples and generate the compression inside the μCT scanner, a motorized holder was designed and manufactured (Fig 2). It is based on a device previously designed to study forced wetting (33). The new design had to provide the specific conditions needed for the tomography, in particular, material transparent to X-rays and the dimensions of the scanner chamber, i.e. 140 mm in height and 75 mm in diameter, which limited the size of the device and therefore the choice of the sensors and actuators.

Basically, in the form of a cylinder–piston combination, the holder was equipped with a linear actuator with a 20 mm maximum stroke and a speed of 0.05 mm.s^{-1} (LAC10A-T4-MC04, Zaber, Canada) and with a miniature load cell with a maximum force of 5 N (XFTC310-5N, TE Connectivity, Switzerland). A circular plunger with a surface area of 2 cm^2 was fixed on the translation stage. To reduce adhesion with the droplet, the plunger was covered with a low surface tension PTFE film.

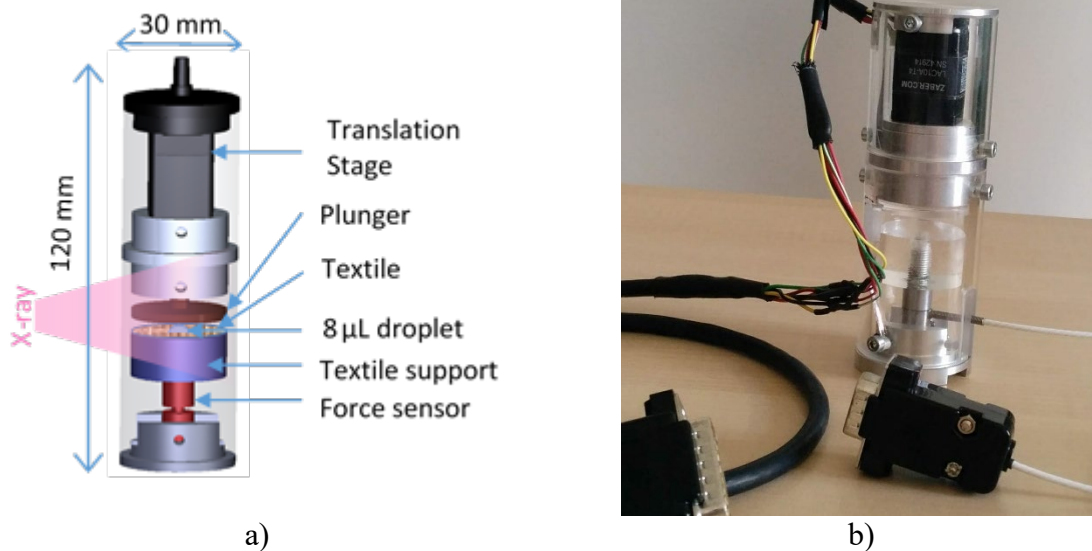


Figure 2: Developed compression device: a) CAD view and b) picture of the system.

The installation set up allowed the movement and the maximum compression force exerted on the droplet/sample to be controlled. The actuator had a resolution of $0.024 \mu\text{m}$ and a unidirectional accuracy of $10 \mu\text{m}$. The acquisition system was an XMCB-1 controller (Zaber, Canada), used both to move the actuator according to the instructions and to acquire the signal from the load cell. Linked to a CDM11 signal conditioner for full bridge sensors, the load cell

had a full scale output of 105.7 mV, but the final resolution of the force acquisition was of 0.025 N in the range of 0 to 10 V. The normal force and plunger displacement with time were recorded.

All the measurements were processed with a maximum force applied of 2 N corresponding to a pressure of 10 kPa under the whole surface of the plunger.

To provide X-ray access to the droplet/textile interface, the cylinder and the plunger were made of PMMA, which has low X-ray attenuation properties for the reduction of the number of artefacts.

Inserting the compression device inside the μ CT scanner in order to perform a time series of projections during compression-decompression required careful placement of the wires (connected to the actuator control unit and the acquisition unit) to avoid visualization problems or mechanical blockage. The compression device had to be installed in the μ CT scanner so that the window was facing the scanner door in order to be able to deposit the water droplet.

2.4 Measurement protocol

In order to have clean borders, the textiles were cut by using laser for cotton samples or ultrasounds for acrylic samples. The samples of 25 mm in diameter was affixed with a thin double-sided adhesive tape onto the support (Fig. 2a). Then, the compression device was carefully introduced into the scanner chamber.

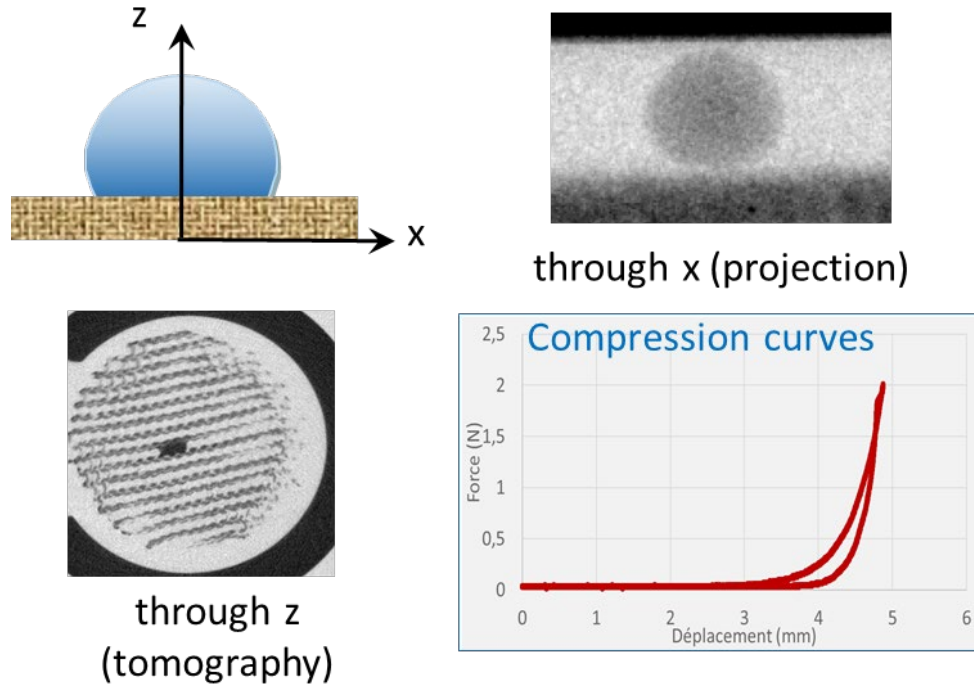


Figure 3: Schema of data obtained from the compression device developed

A droplet of deionized water was deposited onto the textile surface through the window using a dosing pipette. The volume, set at 8 μ L, was a compromise between a relevant amount of water, a negligible gravity effect and to cover at least an elementary pattern of the structure. In fact, the droplet diameter is 2.5 mm which is in the same range of order than the course or wale

lengths for a stitch length of 11.0 mm (with approximately 2 mm/course and 2.2 mm/wale) and larger for a stitch length of 6.8 mm (with approximately 1 mm/course and 1.7 mm/wale).

Due to the quite large fabric thickness (Tab. 1), this amount of water doesn't reach the bottom plate (textile support in Fig. 2a) during compression.

First, a time series of projections was recorded in a vertical median plane during compression of the droplet: this is the 2D projection view. The orientation of the fabric relative to the projection view can be parallel to the course or wale directions. Immediately after the compression test, a 3D tomographic acquisition was processed all around the cylinder. For each fabric investigated at least three samples were tested.

The complete setup mainly provided 2D visualization of the droplet compression/decompression and a tomographic view of the water location after compression (Fig. 3). The force/displacement curves obtained are not interpreted in this study.

3. RESULTS

The first part of the results exposes the method developed to analyze the different measurements obtained from the X-ray imaging consisting in a film (2D projections) and 104 slices (images from tomography) per sample. The second part presents the results from the tests conducted on the 14 distinct knits to consider the influence of several textile parameters (Table 1).

3.1 Droplet visualization and method of analysis

3.1.1 2D visualization of the squeezing dynamic

A dynamic two-dimensional projection offers a visualization of the water migration during a compression-decompression cycle. The location of the liquid in Figure 4 can be tracked by the contrast difference during the test. The depth of the droplet penetration during the test and the profile of the liquid distribution through the textile thickness after the test can be studied.

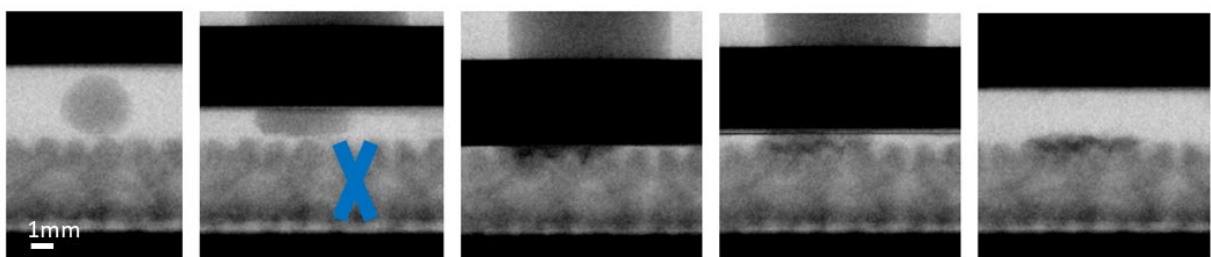


Figure 4: Sequences of compression-decompression of a water droplet on a textile surface (example of sample 1a14-F2 Table 1).

The X shape formed by the loops of an interlock knit, when observed in the wale direction, can be discerned clearly in Figure 4 (drawn in blue in the left-hand picture) (34).

3.1.2 3D visualization of the liquid distribution after compression

The tomographic measurements give an image of the slices of the wetted samples every 74 μm . The wetted zone can be located in each slice by contrast in the grey scale (inside the blue circle in Figure 5).

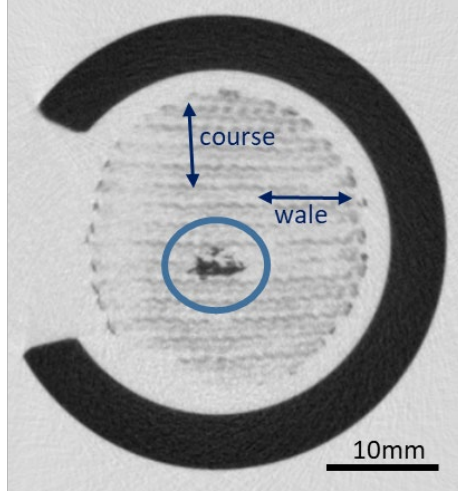


Figure 5: Example of a sectional picture from the tomographic view of the textile after the compression-decompression cycle. The wetted zone is in dark grey inside the blue circle.

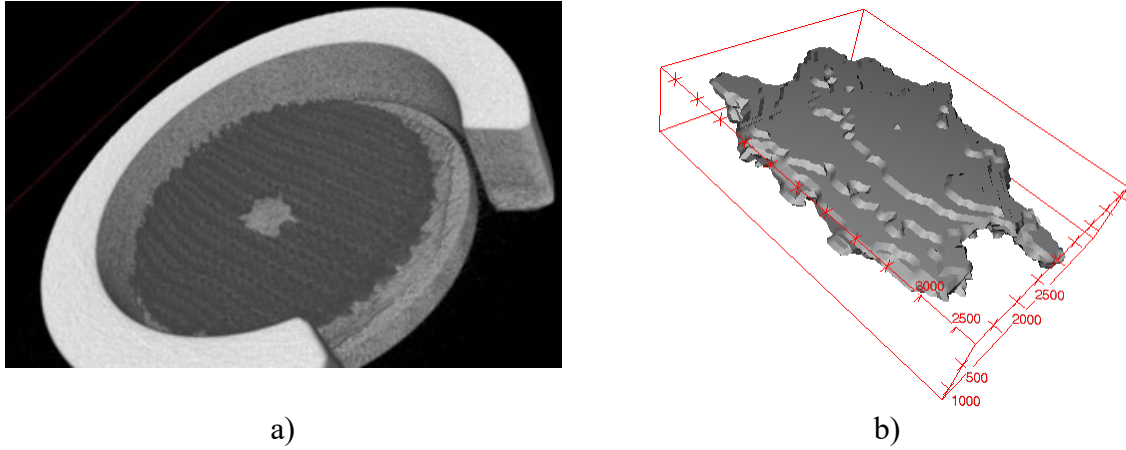


Figure 6: a) 3D reconstruction from the sectional images taken after the compression-decompression cycle, where the liquid zone is in light grey and b) extraction of the droplet shape alone from the 3D reconstruction.

The successive sectional images obtained by the μ CT scanner are assembled using the open source software ImageJ plugin 3D viewer. By choosing a Huang filter and adapting the intensity threshold, the textile and the droplet shape can be selected. A whole 3D reconstruction can be obtained (Fig. 6a) or a droplet extraction (Fig. 6b). The in-plane and transplanar water content can then be evaluated.

3.1.3 Method of analysis of the 3D reconstructed droplet

The fabric parameters, regarding in-plane and transplanar liquid intrusion, are essentially the spreading of the liquid zone, respectively in the fabric surface and in the thickness directions. Therefore, the interesting characteristics of the droplet aspect ratio are its maximum in-plane and transplanar dimensions.

In the method developed in this study, the size of the droplet extracted from the 3D reconstruction is defined from the dimensions of a box strictly containing the drop shape

(Fig. 7a). This box is oriented in the privileged directions according to textile structure, which are the course, wale and thickness directions for knitted textiles. These dimensions are normalized to take into account the variations in droplet volume due to evaporation or sticking to the plunger surface. In fact, each dimension is divided by the cubic root of the final droplet volume, directly calculated from the 3D extraction droplet by ImageJ.

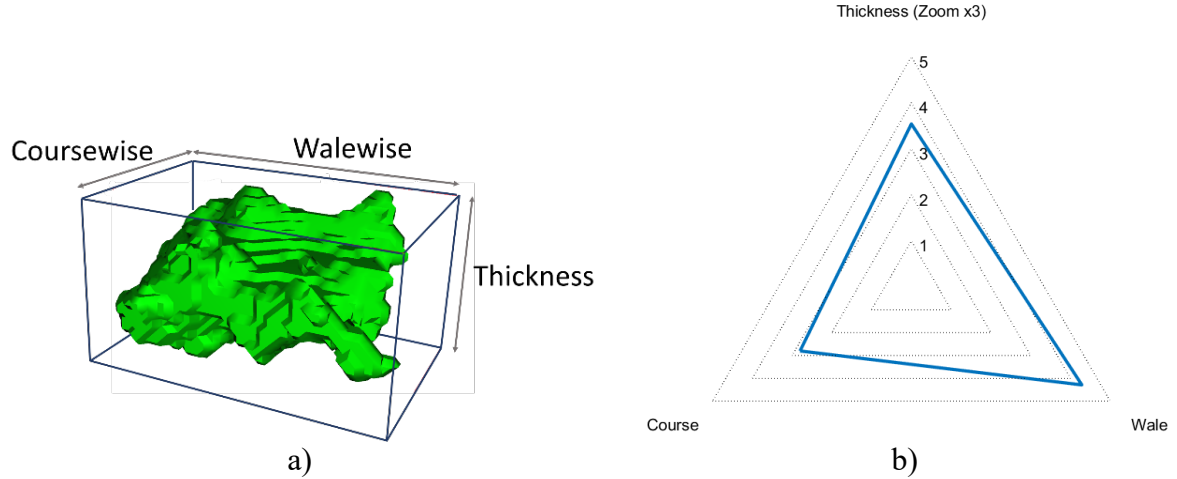


Figure 7: Characteristics of the 3D reconstructed droplet a) the box containing the droplet oriented relative to the fabric structure (course, wale and thickness) and b) chosen representation of these dimensions normalized by the final droplet volume.

The dimensions of the liquid shape, obtained from the 3D reconstruction, are illustrated in three-way charts representing the length (walewise), width (coursewise) and height (in thickness direction) of the box, enabling the visualization of the droplet extensions (Fig. 7b). The thickness scale is multiplied by a factor 3 to obtain an optimized visualization of the thickness variation in these charts.

This method of analysis allows the privileged directions of water dispersion to be highlighted. The triangle area is correlated to the box volume and is indicative of the compactness of the droplet shape.

3.2 Results analysis and influence of the fabric parameters

The influence of the hydrophobic property and the cover factor were analyzed by testing 3 to 8 samples of each of the 14 different knitted fabrics. The CV% is approximately 10% for the thickness dimension and 20% for the course and wale dimensions, which is an expected result for knitted fabrics.

3.2.1 Influence of the hydrophobic chemical treatment

To study the influence of the wetting property, the same textile with and without the hydrophobic chemical treatment described in section 2.1, were tested (respectively fabrics 1b10 and 1a10 in Table 1).

In the case of the slightly hydrophobic samples, droplet fingering was liable to occur (Fig. 8a), and it did not occur with highly hydrophobic treated fabrics (Fig. 8b). The tested fabrics had small inter-yarn pores, i.e. a high cover factor (Table 1), which does not retain water when the surface is superhydrophobic; the liquid mainly spreads at the surface. In the case of slightly hydrophobic fabric, the fingering shows that water penetrates finer pores and remains trapped.

2D visualization before and after compression-decompression shows a more extensive spreading of the droplet in the surface hairiness for superhydrophobic fabrics (Fig. 9).

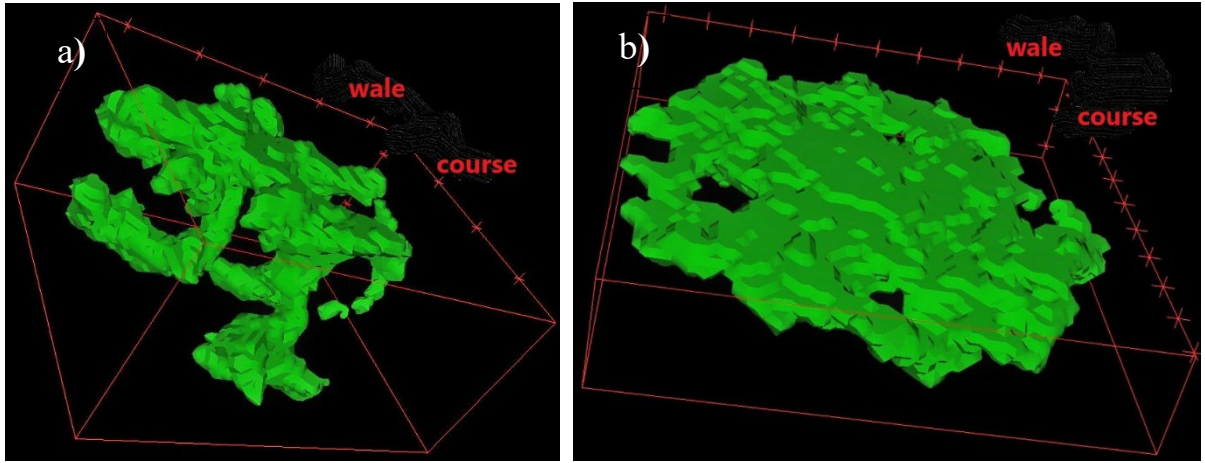


Figure 8: 3D reconstruction of the droplet shape after the compression-decompression test for samples a) slightly hydrophobic (untreated) and b) strongly hydrophobic (treated).

This observation confirms that better water wettability led to higher water retention properties, as observed in the study by Hsieh (35).

Figure 10 shows a quantification of these mechanisms. The droplet spreads preferentially along the wales for the slightly hydrophobic untreated fabric while, on the strongly hydrophobic treated fabric, the expansion of the droplet is balanced in both directions. The penetration thickness after compression appears much larger for the slightly hydrophobic fabric.

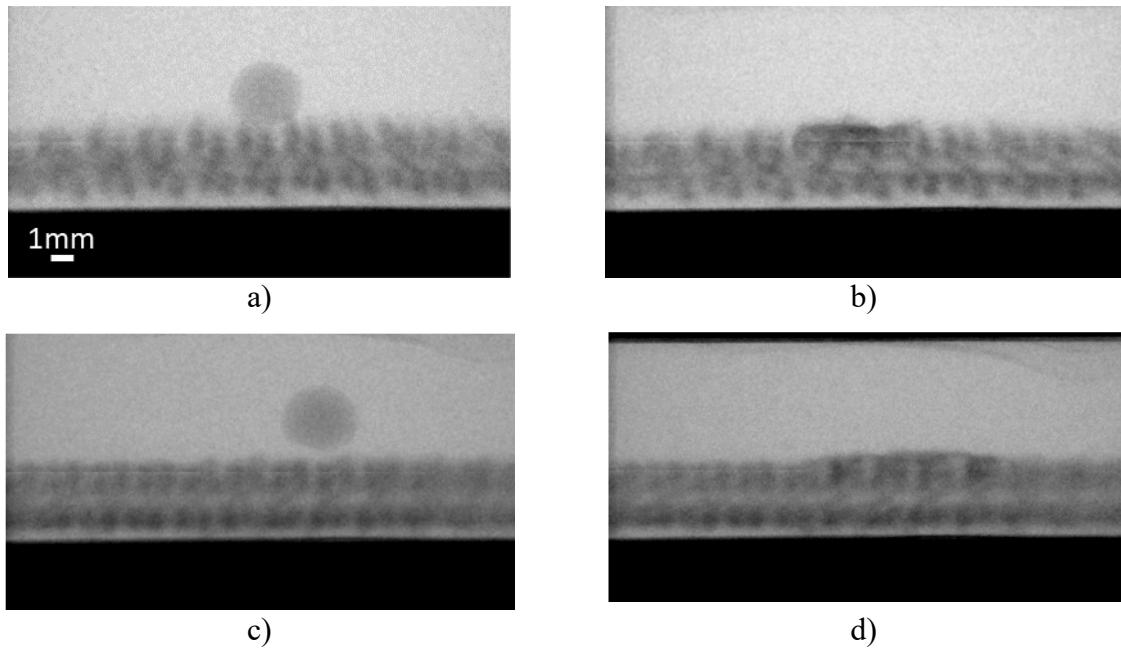


Figure 9: 2D visualization of the droplet for samples a) and b) slightly hydrophobic (untreated) and c) and d) strongly hydrophobic (treated) before (a and c) and after (b and d) the compression-decompression test.

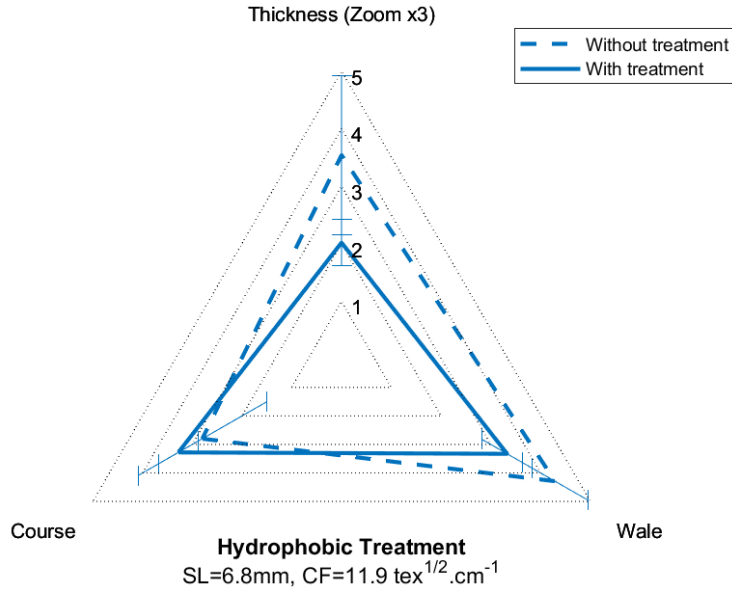


Figure 10: Normalized dimensions of the droplet shape after the compression-decompression test for samples 1a10 and 1b10 made respectively of slightly hydrophobic (without treatment) fabrics and strongly hydrophobic (with treatment) fabrics.

3.2.2 Influence of the cover factor/stitch length

Five samples made of the same acrylic yarn were knitted changing only the stitch length (samples 1a10 of SL=11.9 to 1a14 of SL=7.4 presented in Table 1). The global geometry of the yarns was conserved and a homothetic modification of the pore geometry was made (36). According to Equation 1 when the stitch length increases, the cover factor decreases leading to higher fabric porosity. In this case, the cover factor ranges between 7.3 and 11.9, i.e. a ratio of 1.6 (Table 1).

The 3D reconstruction emphasizes the evolution of the droplet shape with the stitch length (Fig. 11). The emergence of fingering decreases with increasing stitch length and then increasing porosity, and the droplet shape becomes more compact. The tomographic views show that the fingering is driven by the yarns and not the pores due to the stitch shape (Fig. 12). These fingers seem to be due to water trapped within fine pores in the intra-yarn capillaries, i.e. between the fibers.

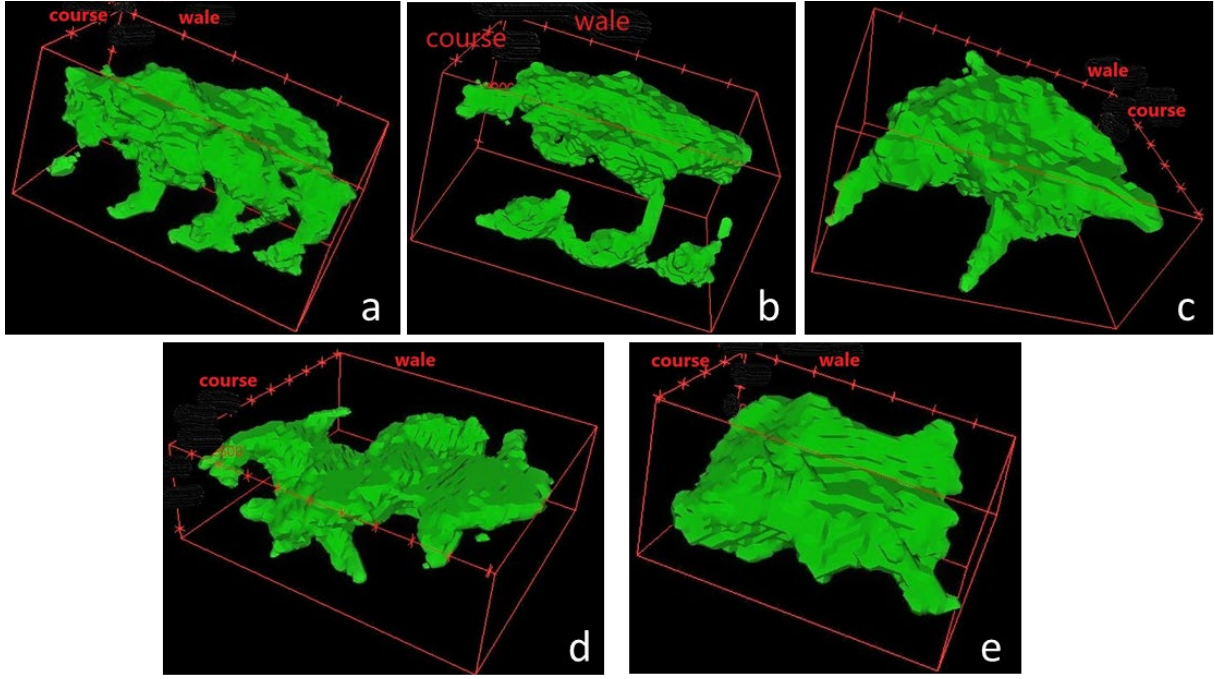


Figure 11: 3D reconstruction of the droplet shape for different stitch lengths and cover factor:
a) SL=6.8 mm and CF=11.9, b) SL=7.8 mm and CF=10.4, c) SL=8.7 mm and CF=9.3, d)
SL=9.9 mm and CF=8.2 and e) SL=11 mm and CF=7.3 (Table 1).

Some yarn-to-yarn liquid transfers were also detected, for example in Figure 11b. In this figure, the fingering shape highlights the liquid path from one yarn to an interlaced yarn through some contact points. Yarn-to-yarn transition for liquid transport inside textile media has already been observed during the wicking process in knitted fabrics (37,38).

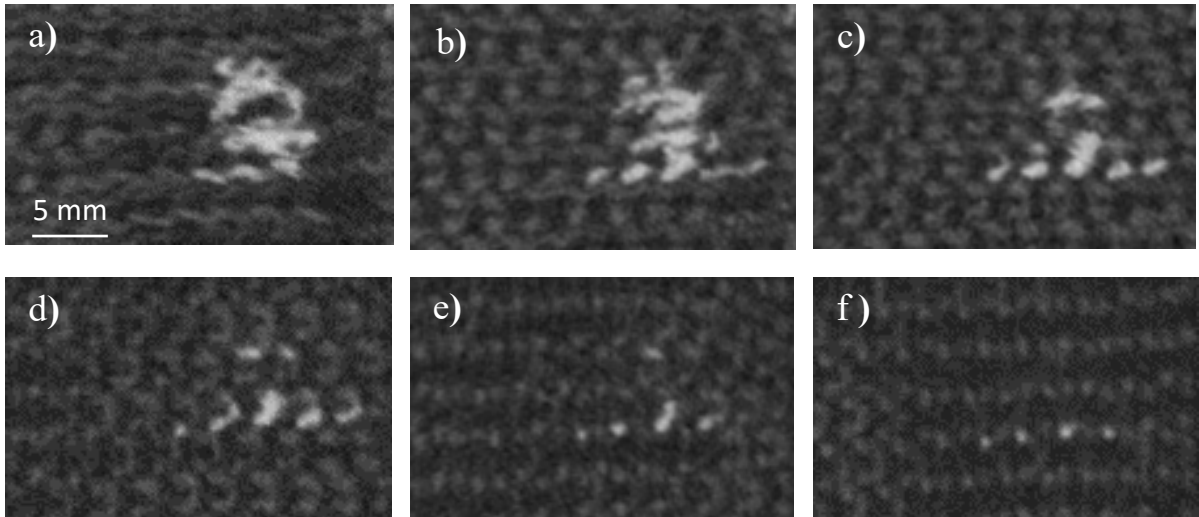


Figure 12: successive tomographic images of the distribution of water (in light grey) inside sample 1a11 (SL=7.8 mm and CF=10.4). Each image in this sequence is separated by 222 μm in depth. The width of the pictures corresponds to the wale direction.

Subsequent projections reveal that the liquid bulk lodges preferentially between two wales, but spreads to neighboring wale valleys when the stitch length becomes too small (Fig. 13 and Fig. 14).

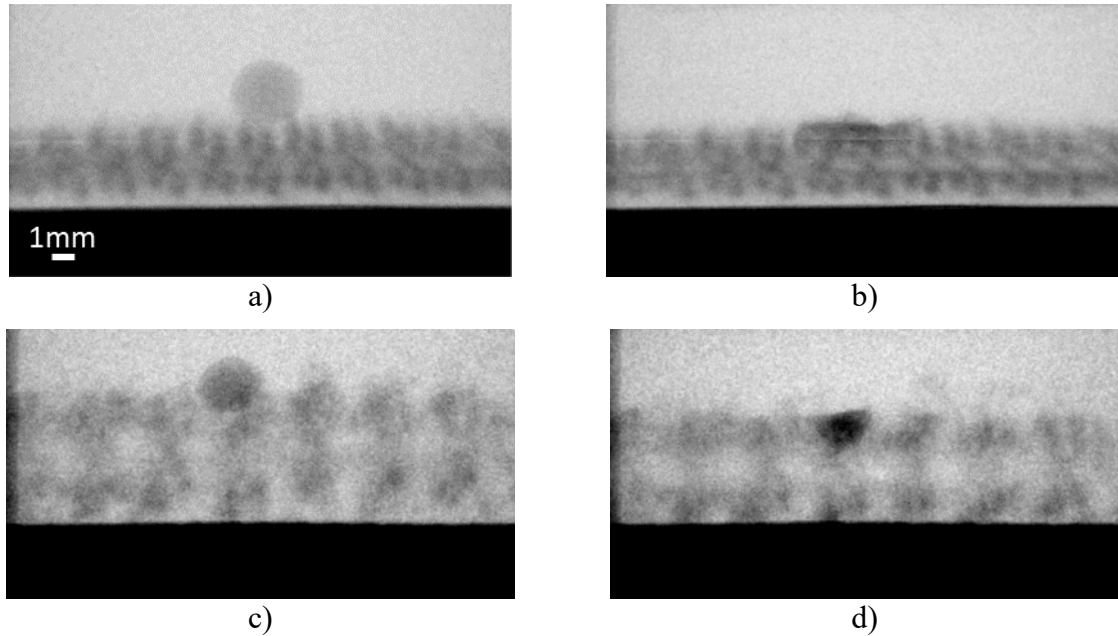


Figure 13: 2D visualization of the droplet for samples a) and b) with a small stitch length and a high cover factor (SL=6.8 mm and CF=11.9) and c) and d) with a large stitch length and a low cover factor (SL=11 mm and CF=7.3) before (a and c) and after the (b and d) compression-decompression test.

The aggregation of these data shows different penetration mechanisms. For large stitch length, the liquid drop fills large channels between yarns, which is typical for such a supply-limited water penetration (39). As stitch length decreases, the space between yarns also decreases and the liquid fills the intra-yarn capillaries.

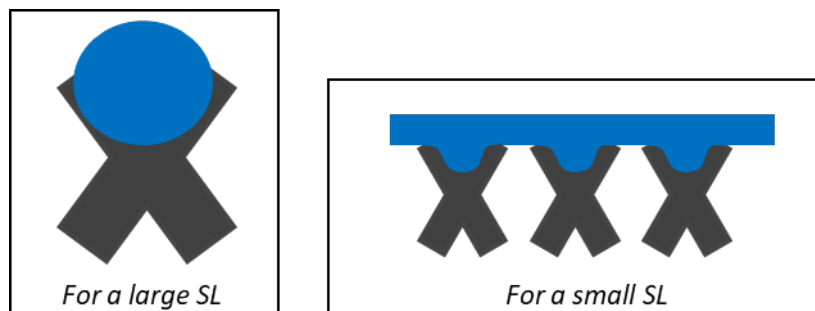


Figure 14: Illustration of water location relative to wales appearing as X shapes for interlock 1 x 1 (Fig. 4).

Figure 15 also illustrates the loss of water droplet compactness when the stitch length decreases. Each triangle of the textile with a smaller stitch length tends to enclose the precedent one, a correlation appears between stitch length and compactness (volume of the box containing the droplet shape) with an R^2 of 0.89.

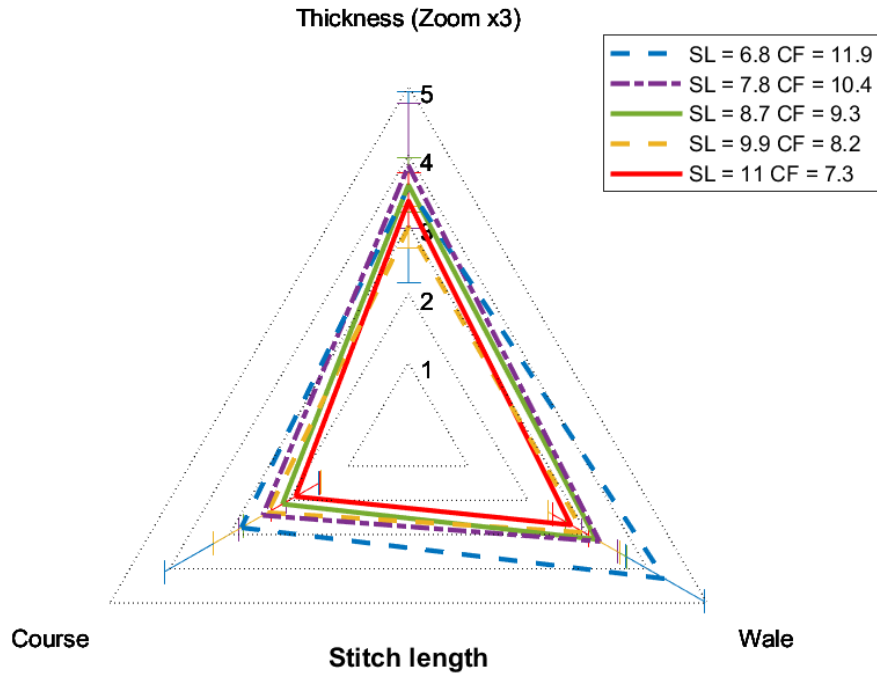


Figure 15: Normalized dimensions of the droplet shape after the compression-decompression test for samples made from the acrylic yarn for different stitch lengths and then cover factors.

3.2.3 Influence of the cover factor/yarn count

The principle used was to increase the yarn count for a fixed stitch length. The cover factor then increases due to an increase in the total yarn count (Eq. 1) and the geometry of the stitch is conserved. Two sets of fabrics were investigated (Table 1): i) set #1 in acrylic (samples 1a12/1a12-F2 and 1a14/1a14-F2 and ii) set #2 in cotton (4b10-F1 to F3).

The 3D reconstructions are illustrated in Figure 16 for set #2.

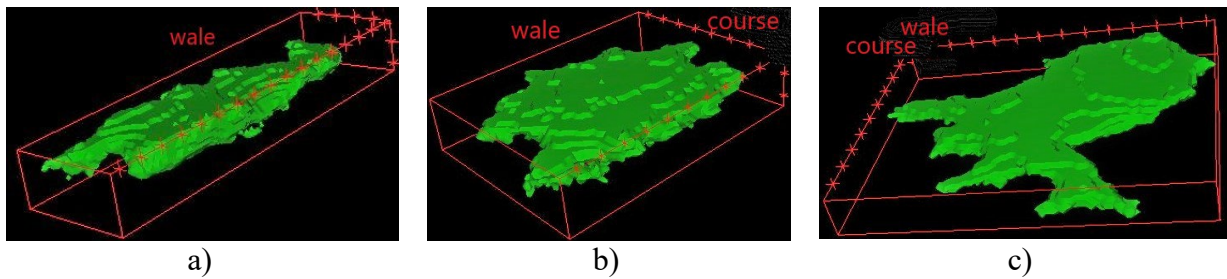


Figure 16: 3D reconstruction of the droplet shape for samples knitted a) with one yarn (CF=7.9), b) two yarns (CF=11.1) and c) 3 yarns (CF=13.6) after the compression-decompression test.

The increasing cover factor limits the penetration thickness and promotes spread along the coursewise direction (Fig. 17). In this case, the cover factor ratio is approximately 1.4, whatever the fabric couple (Table 1).

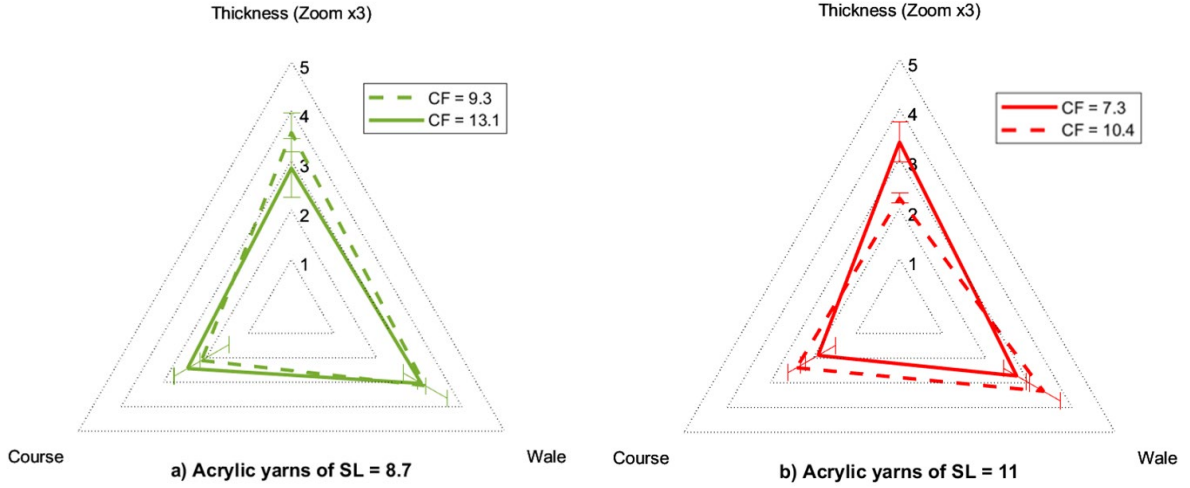


Figure 17: Normalized dimensions of the droplet shape after the compression-decompression test for set #1 samples made from 1 and 2 acrylic yarns for 2 different stitch lengths: a) SL=8.7 mm and b) SL=11 mm (Table 1).

The same tendency is also visible in Figure 18 for the cotton samples knitted with 1, 2 or 3 yarns with the same stitch length (respectively samples 4b10-F1, F2 and F3, Table 1). Moreover, for this set of fabrics the liquid spread also takes place in the walewise direction, which was less visible in the results presented in Figure 17. In this case, the cover factor range is from 7.9 to 13.6, i.e. a ratio of approximately 1.7 (Table 1).

Changing the cover factor at constant stitch geometry seems to induce variations in droplet spreading in the three directions.

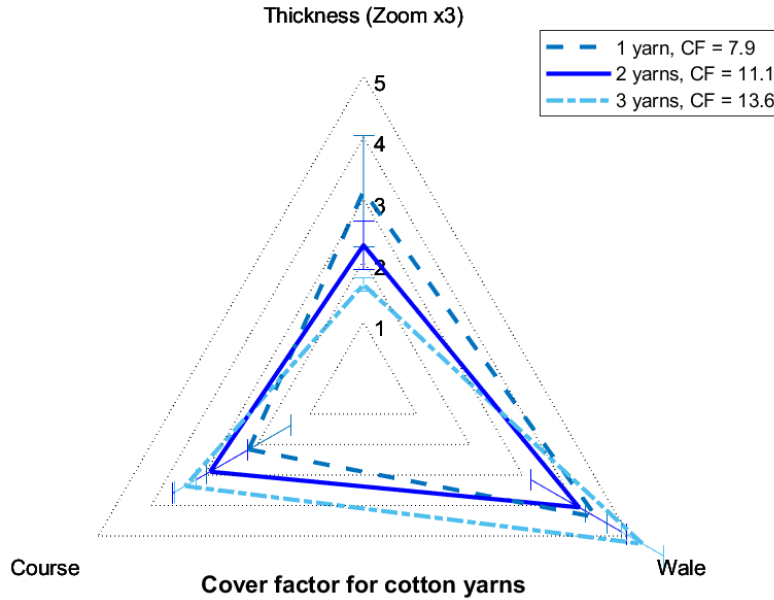


Figure 18: Normalized dimensions of the droplet shape after the compression-decompression test for set #2 hydrophobic treated samples made from 1, 2 or 3 cotton yarns for a fixed stitch length (Table 1).

3.2.4 Fixed cover factor with different stitch lengths and yarn count

The cover factor is an important parameter in penetration behavior. In this section, the goal was to keep the same kind of knit and the same cover factor while changing both stitch length and yarn count. Fabrics 1a11 and 1a14-F2, which have a cover factor of 10.4 (Table 1) are compared. Figure 19 illustrates the difference in material density in both fabrics.

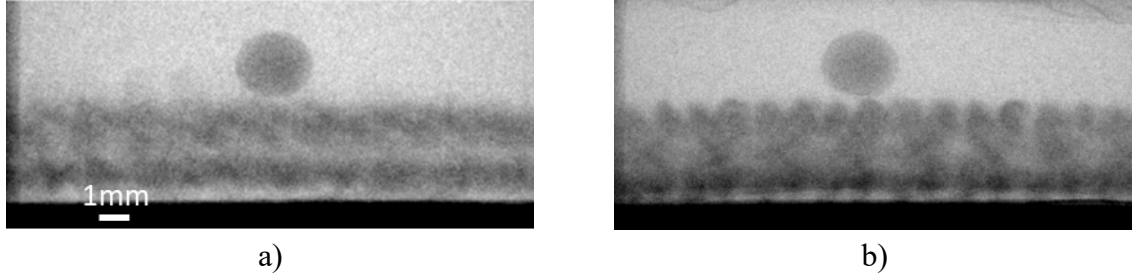


Figure 19: 2D visualization of the droplet for samples with the same cover factor (CF=10.4)
a) with a yarn count of 65 tex and a stitch length of 7.8 mm, b) with a total yarn count of 130 tex and a stitch length of 11 mm.

The results obtained shown a distinct penetration thickness, for similar spreading the coursewise and walewise directions (Fig. 20).

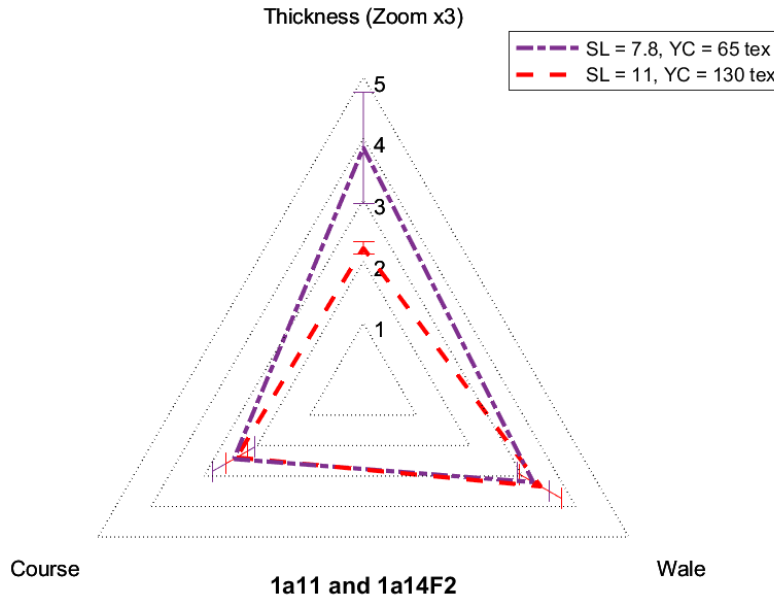


Figure 20: Normalized dimensions of the droplet shape after the compression-decompression test for samples with same cover factor (CF=10.4) but with different stitch lengths and yarn counts (Table 1).

3.2.5 Influence of the kind of knit

Complementary trials were carried out changing the kind of knit, then the structure and the surface texture.

Knits P1 and P2 were very similar as shown in Table 2. It can be confirmed by the structure geometry as revealed in Figure 21 meanwhile that droplet shape after compression-decompression differs drastically, as shown in Figure 22. The factors affected here are mainly impregnation thickness and walewise expansion.

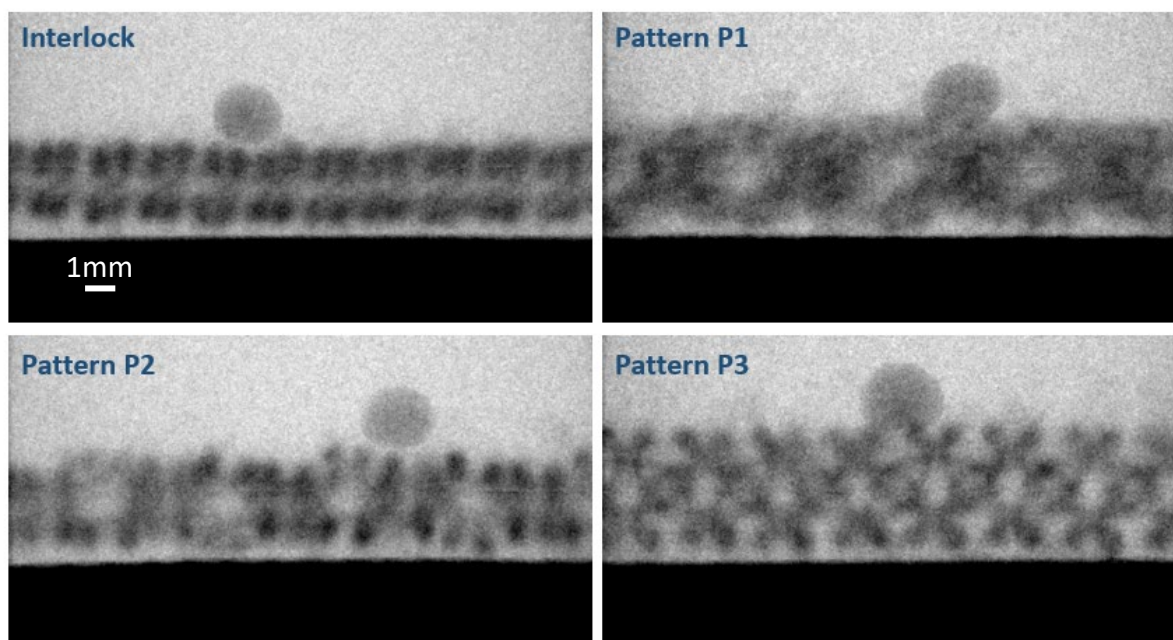


Figure 21: 2D visualization of a droplet deposited on 4 samples with same stitch length and different kinds of knit.

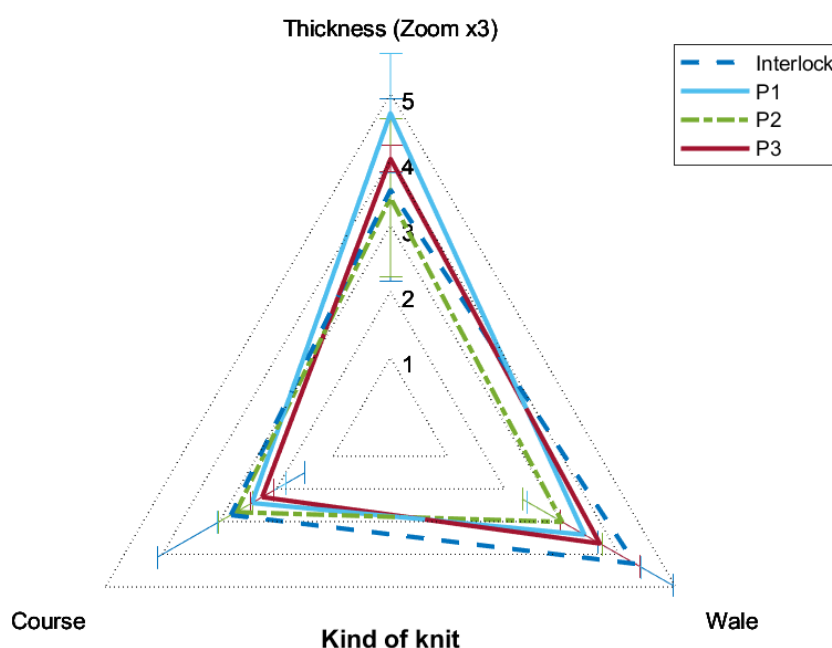


Figure 22: Dimensions of the droplet shape after the compression-decompression test for samples made from different kinds of knit with the same stitch length (Table 1)

4. DISCUSSION

4.1 On the influence of the fabric parameters

The 14 different knitted samples allowed an analysis of the influence of the following parameters: the hydrophobic property, fiber material, stitch length, cover factor and kind of knit. Therefore, these fabrics had different levels of hydrophobicity and multiscale porosity. As was shown in section 3.2, the two most important parameters for water penetration into a textile structure are its level of hydrophobicity and pore size. This tends to corroborate some results indicating that the factors determining the liquid pressure required to enter a hydrophobic fibrous network are the wettability of the material (9) and the pore size (11).

The chemical treatment modified the initial properties of the two materials used, i.e. acrylic and cotton, turning them into hydrophobic materials. The acrylic fabrics were compared before and after this treatment (section 3.2.1) and all the cotton fabrics used were treated (section 3.2.3). For all the fabrics investigated in this study, before compression, the droplet presented a contact angle much higher than 90° at the textile surface, as can be seen, for instance, in Figures 9 and 19.

The influence of porosity at yarn scale (27), i.e. between the fibers or intra-yarn, was not investigated in this study because the fabrics compared were made of the same yarn. Porosity at fabric structure scale, i.e. inter-yarn, was modified in two different ways: by varying stitch length for the same yarn or by varying the number of yarns for the same stitch length. This porosity can be evaluated in a first approach with the cover factor: the higher the cover factor, the lower the porosity (Table 1).

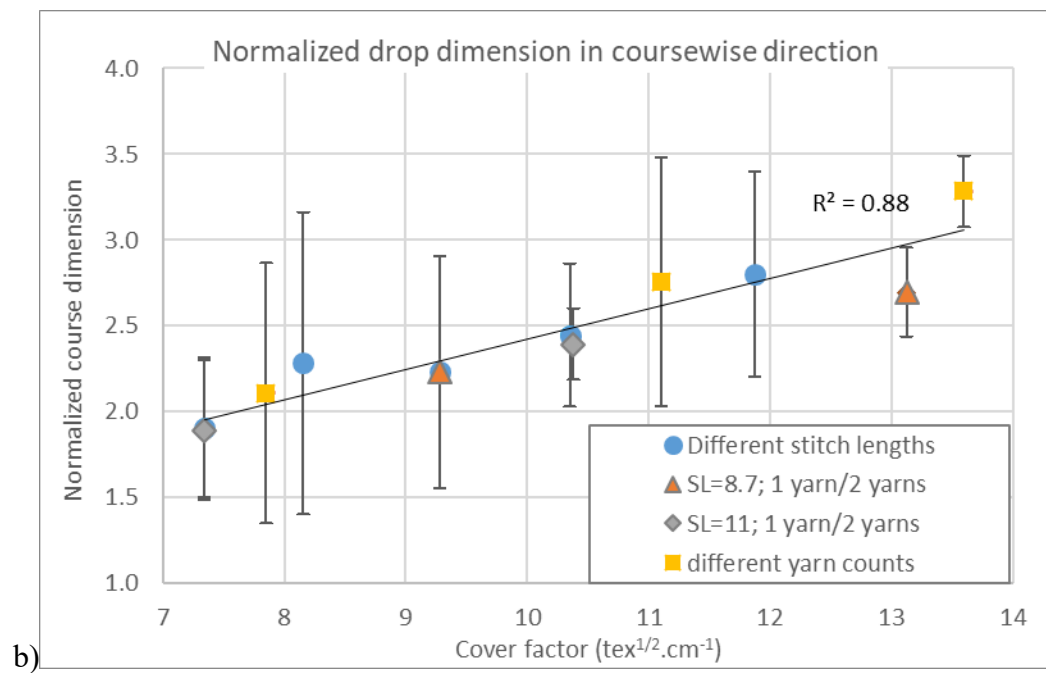
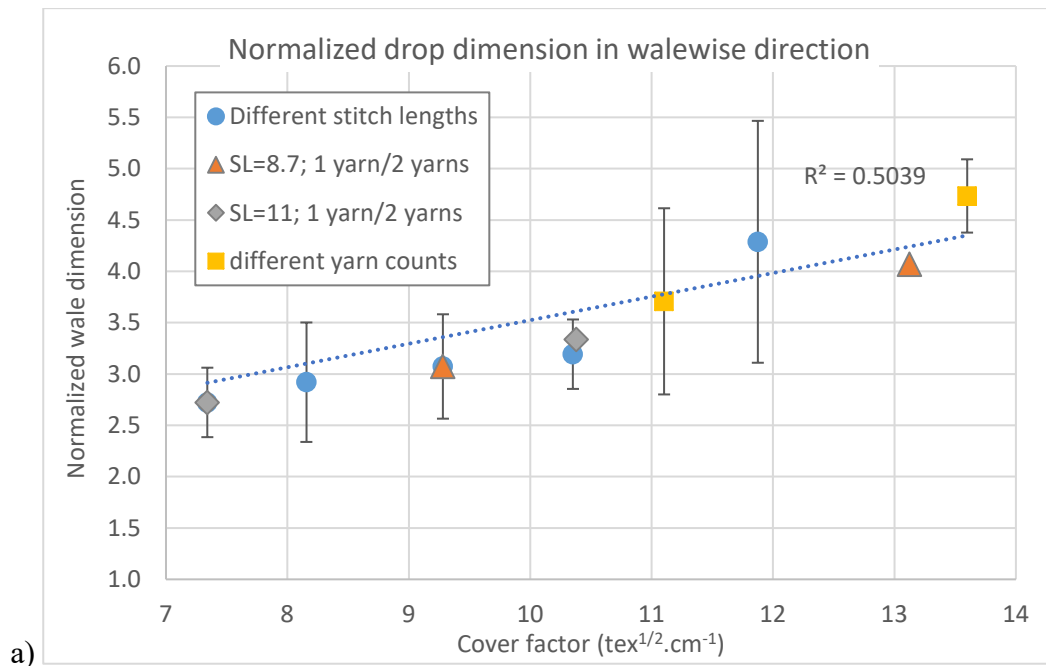
In this study, a droplet is first placed on the textile surface, therefore the liquid volume is small, and it corresponds to a different case to an infinite reservoir.

The droplet spreading on and inside the structure was quantified after compression-decompression by measuring the dimensions of the droplet in 3 directions (wale, course and thickness), and the fluid dynamics were observed from qualitative point of view by 2D projection.

4.1.1 On the influence of the cover factor

The influence of the fabric cover factor was noticeable whatever the method used, by changing the stitch length (section 3.2.2.) or the total yarn count (section 3.2.3). According to the results obtained, when the cover factor increases, i.e. when the porosity decreases, the transplanar liquid penetration decreases, favoring in-plane spreading (Fig. 15, 17, 18). It seems that changing the cover factor in the same range 1.6 and 1.7 is not equivalent if stitch length or yarn count are modified. In fact, stitch length influence in-plane spreading more (Fig. 15), whereas a change in yarn count changes both in-plane and transplanar spreading (Fig. 18). Changing both of them while maintaining the cover factor (section 3.2.4) influences transplanar spreading, showing a change in the pore geometry (Fig. 20).

From a global point of view, for a given knit pattern, the expansion of the droplet of liquid monotonically increases with the cover factor in the planar directions (Fig. 23 a and b). For the samples considered in this study, a linear correlation ($R^2=0.88$) appears for the normalized course dimension (Fig. 23b). For the wale direction, the relationship is less clear ($R^2=0.50$). No specific trend was observed in the transplanar direction (Fig. 23c).



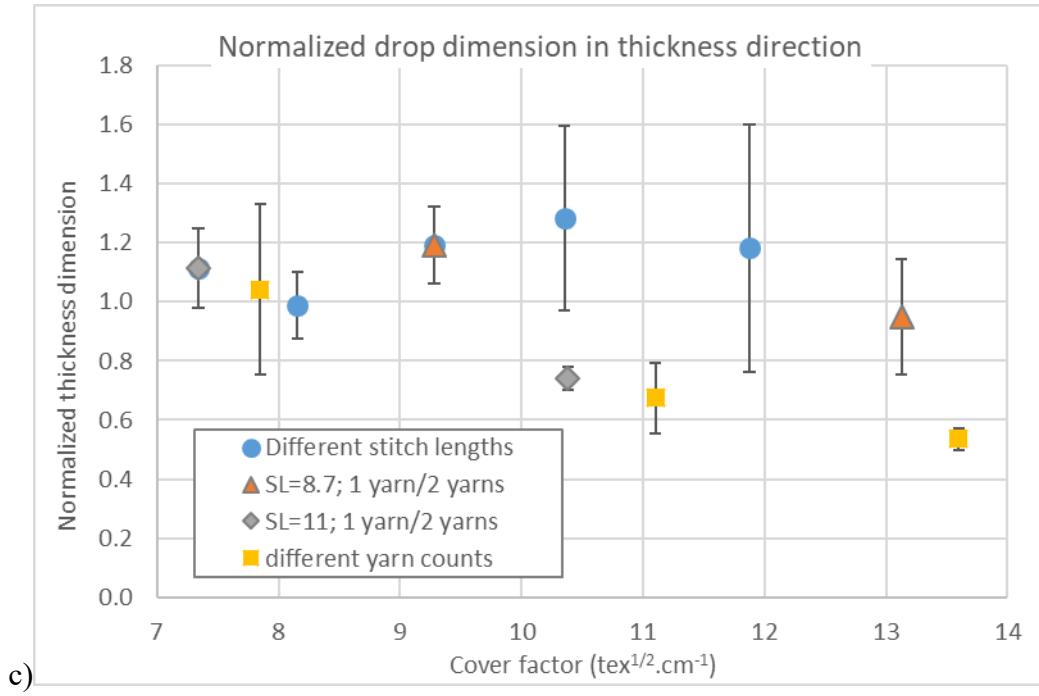


Figure 23: Influence of the cover factor on the non-dimensionalized lengths of the humid shape in the a) wale, b) course and c) thickness directions.

4.1.2 On the combined influence of cover factor and hydrophobicity

Two identical structures with a high cover factor (CF=11.9), i.e. with low porosity, were compared before and after hydrophobic treatment (section 3.2.1). A preferred direction of spreading appeared along the wale for the untreated sample (Fig. 10), while the treated sample showed no preferred direction. At constant water volume, the untreated fabric generated a less compact and more deeply trapped liquid shape inside the textile sample than the highly hydrophobic fabric, probably due to some liquid invading the thinner voids (intra-yarn capillaries) (39). However, during compression, it was observed that the water deeply penetrated the treated fabric, mainly filling the structure pores (inter-yarn voids) before re-covering the surface at the end of the compression. For textile structures with a low cover factor, intra-yarn invasion should be less significant because the inter-yarn pores are more important for water spreading. As a practical implication, a single layer of a liquid-repellent textile is thus not sufficient to obtain a liquid-protective fabric under the action of applied pressure. The usual use of multi-layer materials is needed to halt liquid penetration (22).

A decrease in porosity, i.e. an increase in the cover factor, modifies the privileged directions of spread by increasing expansion in the walewise and coursewise directions (Fig. 15 and Fig. 18) and/or by decreasing penetration into the thickness (Fig. 17 and Fig. 18).

For spontaneous wicking following droplet deposition in non-hydrophobic textiles, the process mainly starts with a liquid penetration, that is a liquid transport normal to the plane of the textile, which is followed by in-plane spreading (40). Here, during the forced migration of the deposited droplet, the first stage mainly consisted in spreading on the surface for hydrophobic structures, and then the liquid penetrated through the thickness. After decompression, no wicking was

observed; the liquid either remained trapped inside the textile structure or partly moved back to the surface.

Among the geometric textile variables, the cover factor appears to be predominant for in-plane liquid expansion. Increased density in the knitting construction promotes lateral dispersion as was hypothesized in (29). The transverse penetration mechanism could not be directly attributed to a specific material parameter and revealed different mechanisms according to the pore structure. Liquid invasion privileged inter-yarn pores for large stitch lengths and took a path through inter-fiber pores for small stitch lengths.

From a global point of view, in-plane expansion can be tuned by the cover factor, the higher it is the better is in-plane spreading, whatever the method used to change it. However, transplanar spreading seems less related to the cover factor: it is decreased by hydrophobic chemical treatment (Fig. 10) or by using a coarser yarn, i.e. by decreasing pore size due to the stitch shape (Fig. 17, 18 and 20).

4.2 On the method of analysis

X-ray imaging enables non-invasive quantitative monitoring of liquid dispersion within opaque fabrics with a complex pore structure. The in-plane spreading can be analyzed, and privileged directions are highlighted. The quantity of liquid as a function of thickness is also accessible. This method is a 3D generalization of the usual methods mentioned in the introduction of evaluating liquid retention and barrier performance against liquid penetration. The usual tests often give 2D information for in-plane liquid spreading (capillary rise method, moisture management tester, etc.) or the transverse property (spontaneous wettability or forced wet-through tests). Here, the 3D information is achieved by taking into account the shape of the liquid zone inside the fabric.

The textile was also imaged so that the intrusion of the liquid droplet could be observed whilst external pressure was applied. This test is complementary to the usual imaging tests dedicated to the study of spontaneous wicking behavior in hydrophilic fabrics (22–31). The property available for evaluation is fabric wet-through robustness, for example to prevent surgeons or firefighters from liquid contaminants.

The exploitation of the presented results, mainly via the maximum lengths of the liquid dispersion in the three directions (walewise, coursewise and transversal), depends on the fabric's practical uses and the textile process parameters. For conductive inkjet printing, for example, the in-plane ink dimensions must ensure the neighboring coalescence to provide a conductive path. However, these dimensions are expected to guarantee the required print definition. The penetration depth must be large enough to obtain good adhesion of the ink on the fabric while optimizing the quantity of dispensed ink.

The triangle diagramming of these dimensions chosen here highlights the maximum expansion of the liquid inside the textile structure in the privileged direction corresponding to the walewise, coursewise or transverse direction. The number of fingers or quantity of liquid present at the maximum wet-depth is lacking to provide a complete description of the results.

Optimizing the resolution of the tomographic images obtained, as described in (23), should provide a finer understanding of the phenomena at play.

5. CONCLUSION

This study presents a new method using X-ray imaging and tomography to study the complex forced water spreading behavior of hydrophobic textiles with different geometrical characteristics.

This study focused on the liquid penetration driven by an applied compressive load. It should be emphasized that it followed a different dynamic from liquid penetration driven by capillary pressure alone, which is termed “wicking”. Understanding within-a-yarn and yarn-to-yarn wicking within a fabric is a first step towards predicting liquid movement inside textile structures. Meanwhile considering water distribution in fabrics during and after compression is key to predicting the robustness of a textile barrier vs liquid penetration.

Hydrophobic treatment was shown to minimize water retention properties, but did not inhibit transverse water penetration during compression.

This study showed that future measurements in real-time two-dimensional radiography during compression could be sufficient to identify the in-plane and transplanar water distribution. In particular, the water remaining in the hydrophobic structure after the end of the compression should be analyzed in more detail in future work.

Acknowledgments

The authors are deeply grateful to Brigitte Camillieri, assistant professor at the University of Haute Alsace for manufacturing the knitted fabrics. The author thanks Philippe Kunemann for the measurement of yarn wetting properties. This research was partly supported by a PHC French-Swiss grant [no. 46577ZL].

Reference list

1. Minor FW, Schwartz AM, Wulkow EA, Buckles LC. The Migration of Liquids in Textile Assemblies: Part II: The Wicking of Liquids in Yams. *Text Res J.* 1959 Dec;29(12):931–9.
2. Kissa E. Wetting and Wicking. *Text Res J.* 1996 Oct 1;66(10):660–8.
3. Perwuelz A, Mondon P, Caze C. Experimental Study of Capillary Flow in Yarns. *Text Res J.* 2000 Apr 1;70(4):333–9.
4. Sharabaty T, Biguenet F, Dupuis D, Viallier P. Investigation on moisture transport through polyester/cotton fabrics. *IJFTR Vol334 Dec 2008* [Internet]. 2008 Dec [cited 2021 Sep 24]; Available from: <http://nopr.niscair.res.in/handle/123456789/2603>
5. Minor FW, Schwartz AM, Buckles LC, Wulkow EA, Marks MP, Fielding GH. The Migration of Liquids in Textile Assemblies: Part IV: Penetration of Fabrics by Liquids. *Text Res J.* 1961 Jun;31(6):525–39.

6. Tang K, Wu Y, Chau KH, Kan C, Fan J. Characterizing the transplanar and in-plane water transport of textiles with gravimetric and image analysis technique: Spontaneous Uptake Water Transport Tester. *Sci Rep*. 2015 Apr 15;5:9689.
7. Parada M, Derome D, Rossi R, Carmeliet J. A review on advanced imaging technologies for the quantification of wicking in textiles. *Text Res J*. 2017 Jan 1;87(1):110–32.
8. Cotorobai VF, Zgura I, Birzu M, Frunza S, Frunza L. Wicking behavior of fabrics described by simultaneous acquiring the images of the wet region and monitoring the liquid weight. *Colloids Surf Physicochem Eng Asp*. 2016 May 20;497:146–53.
9. Miller A, Schwartz P. A Test Methodology for Studying Liquid Penetration of Barrier Materials. *Text Res J*. 2000 Jan;70(1):77–83.
10. Hu J, Li Y, Yeung KW, Wong ASW, Xu W. Moisture Management Tester: A Method to Characterize Fabric Liquid Moisture Management Properties. *Text Res J*. 2005 Jan 1;75(1):57–62.
11. Unsal E, Dane JH, Schwartz P. Effect of liquid characteristics on the wetting, capillary migration, and retention properties of fibrous polymer networks. *J Appl Polym Sci*. 2005 Jul 5;97(1):282–92.
12. Washburn EW. The Dynamics of Capillary Flow. *Phys Rev*. 1921 Mar 1;17(3):273–83.
13. de Gennes PG, Brochard-Wyart F, Quéré D. Hydrodynamics of Interfaces: Thin Films, Waves, and Ripples. In: de Gennes PG, Brochard-Wyart F, Quéré D, editors. *Capillarity and Wetting Phenomena: Drops, Bubbles, Pearls, Waves* [Internet]. New York, NY: Springer New York; 2004. p. 107–38. Available from: https://doi.org/10.1007/978-0-387-21656-0_5
14. Jazia DB, Vonna L, Knopf S, Schrodj G, Nouali H, Lebeau B, et al. Absorption of water/ethanol microdroplets into model porous networks. *Colloids Surf Physicochem Eng Asp*. 2013 Sep 5;436:363–70.
15. Lundberg A, Örtengren JÖ, Alfthan E, Ström G. Paper-ink interactions: Microscale droplet absorption into paper for inkjet printing. *Nord Pulp Pap Res J*. 2011 Jan 1;26(1):142–50.
16. Hsieh YL. Liquid Transport in Fabric Structures. *Text Res J*. 1995 May 1;65(5):299–307.
17. Duprat C. Moisture in Textiles. *Annu Rev Fluid Mech*. 2022;54(1):443–67.
18. Lamminmäki TT, Kettle JP, Puukko PJT, Ridgway CJ, Gane PAC. Short timescale inkjet ink component diffusion: An active part of the absorption mechanism into inkjet coatings. *J Colloid Interface Sci*. 2012 Jan 1;365(1):222–35.
19. Melki S, Biguenet F, Dupuis D. Hydrophobic properties of textile materials: robustness of hydrophobicity. *J Text Inst*. 2019 Aug 3;110(8):1221–8.
20. Tang KPM, Chau KH, Kan CW, Fan JT. Characterizing the transplanar and in-plane water transport properties of fabrics under different sweat rate: Forced Flow Water Transport Tester. *Sci Rep*. 2015 Nov 23;5(1):17012.

21. Kim I, Ju B, Zhou Y, Li BM, Jur JS. Microstructures in All-Inkjet-Printed Textile Capacitors with Bilayer Interfaces of Polymer Dielectrics and Metal–Organic Decomposition Silver Electrodes. *ACS Appl Mater Interfaces*. 2021 May 26;13(20):24081–94.
22. Bencsik M, Adriaensen H, Brewer SA, McHale G. Quantitative NMR monitoring of liquid ingress into repellent heterogeneous layered fabrics. *J Magn Reson*. 2008 Jul 1;193(1):32–6.
23. Blunt MJ, Bijeljic B, Dong H, Gharbi O, Iglauer S, Mostaghimi P, et al. Pore-scale imaging and modelling. *Adv Water Resour*. 2013 Jan 1;51:197–216.
24. Park SJ, Weon BM, Lee JS, Lee J, Kim J, Je JH. Visualization of asymmetric wetting ridges on soft solids with X-ray microscopy. *Nat Commun*. 2014 Jul 10;5(1):4369.
25. Lin Q, Bijeljic B, Berg S, Pini R, Blunt MJ, Krevor S. Minimal surfaces in porous media: Pore-scale imaging of multiphase flow in an altered-wettability Bentheimer sandstone. *Phys Rev E*. 2019 Jun 10;99(6):063105.
26. Yoiti Ito Parada M, Matthias Schlepütz C, Michel Rossi R, Derome D, Carmeliet J. Two-stage wicking of yarns at the fiber scale investigated by synchrotron X-ray phase-contrast fast tomography. *Text Res J*. 2019 Dec 1;89(23–24):4967–79.
27. Fischer R, Schlepütz CM, Hegemann D, Rossi RM, Derome D, Carmeliet J. Four-dimensional imaging and free-energy analysis of sudden pore-filling events in wicking of yarns. *Phys Rev E*. 2021 May 10;103(5):053101.
28. Stämpfli R, Brühwiler PA, Rechsteiner I, Meyer VR, Rossi RM. X-ray tomographic investigation of water distribution in textiles under compression – Possibilities for data presentation. *Measurement*. 2013 Apr 1;46(3):1212–9.
29. Rossi RM, Stämpfli R, Psikuta A, Rechsteiner I, Brühwiler PA. Transplanar and in-plane wicking effects in sock materials under pressure. *Text Res J*. 2011 Sep 1;81(15):1549–58.
30. Sinchuk Y, Pannier Y, Gueguen M, Tandiang D, Gigliotti M. Computed-tomography based modeling and simulation of moisture diffusion and induced swelling in textile composite materials. *Int J Solids Struct*. 2018 Dec 1;154:88–96.
31. Larson NM, Zok FW. Insights from in-situ X-ray computed tomography during axial impregnation of unidirectional fiber beds. *Compos Part Appl Sci Manuf*. 2018 Apr 1;107:124–34.
32. Postle R, Carnaby GA, Jong S. Chapter 10: The plain-knitted structure. In: *The mechanics of wool structures*. Chichester: Dr. D. H. Sharp; 1988. p. 227–73. (Ellis Horwood Limited).
33. Melki S, Biguenet F, Dupuis D. Hydrophobic properties of textile materials: robustness of hydrophobicity. *J Text Inst*. 2019 Jan 2;1–8.
34. Postle R, Carnaby GA, De Jong S. The mechanics of wool structures. 19880000 [cited 2021 Oct 1]; Available from: <https://www.bcin.ca/bcin/detail.app?id=92897>
35. Hsieh YL. Liquid Transport in Fabric Structures. *Text Res J*. 1995 May 1;65(5):299–307.

36. Munden DL. The geometry and dimensional properties of plain-knit fabrics. *J Text Inst Trans.* 1959 Jul 1;50(7):T448–71.
37. Kim H sang, Michielsen S, DenHartog E. New wicking measurement system to mimic human sweating phenomena with continuous microfluidic flow. *J Mater Sci.* 2020 Jun 1;55(18):7816–32.
38. Fischer R, Schlepütz CM, Rossi RM, Derome D, Carmeliet J. Wicking through complex interfaces at interlacing yarns. *J Colloid Interface Sci.* 2022 Nov 15;626:416–25.
39. Birrfelder P, Dorrestijn M, Roth C, Rossi RM. Effect of fiber count and knit structure on intra- and inter-yarn transport of liquid water. *Text Res J.* 2013 Sep;83(14):1477–88.
40. Zhang G, Parwani R, Stone CA, Barber AH, Botto L. X-ray Imaging of Transplanar Liquid Transport Mechanisms in Single Layer Textiles. *Langmuir.* 2017 Oct 31;33(43):12072–9.